Aerosol and Air Quality Research, 18: 2173–2184, 2018

ISSN: 1680-8584 print / 2071-1409 online
doi: 10.4209/aaqr.2017.10.0398

Meteorological Overview and Signatures of Long-range Transport Processes during the MAPS-Seoul 2015 Campaign

Cheol-Hee Kim[1*], Hyo-Jung Lee[1], Jeong-Eon Kang[1], Hyun-Young Jo[1], Shin-Young Park[1], Yu-Jin Jo[1], Jong-Jae Lee[1], Geum-Hee Yang[1], Taehyun Park[2], Taehyoung Lee[2]

[1] *Department of Atmospheric Sciences, Pusan National University, Busan 46241, Korea*
[2] *Department of Environmental Science, Hankuk University of Foreign Studies, Yongin 17035, Korea*

ABSTRACT

During the Megacity Air Pollution Studies-Seoul (MAPS-Seoul) 2015 campaign, which was conducted from May 27 to June 13, 2015, as a pilot for the Korea-US Air Quality (KORUS-AQ) 2016 campaign, seven flights were conducted around the west coast of the Korean Peninsula, the Yellow Sea, the Seoul metropolitan area, and several urban/suburban areas in South Korea. Signatures of the long-range transport processes over Northeast Asia were then summarized from the following: 1) the presentation of a brief description of the synoptic situation for each of the seven flight missions, from RF1 to RF7; 2) interpretations of both streamline and trajectory analyses that described the meteorological history of an air mass; and 3) the calculation of 17 meteorological parameters, including the geostrophic wind speed, the vorticity at a geopotential height of 850 hPa, and several vertical stability indices.

The synoptic conditions during the campaign period were characterized by migratory cyclones and anticyclones with appropriate streamlines and backward trajectories over Northeast Asia. The "stagnant" case was characterized by weak geostrophic wind speed, smaller vorticity, and lower humidity atmospheric conditions, whereas the "long-range transport" case had higher geostrophic wind speed, positive vorticity, and higher humidity atmospheric conditions. Among the seven flights, RF1 and RF2 were identified as dominant stagnant synoptic cases from several diagnostic variables, while long-range transport processes were observed in RF3, RF6, and RF7. RF4 found two mixed characteristics, an upper atmosphere with long-range transport processes and a lower atmosphere characterized by stagnant conditions, and RF5 showed a transport pattern from the southern marine atmosphere without long-range transport from the high emission area. Other meteorological features were also discussed in association with the signatures of the long-range transport processes occurring over Northeast Asia during the MAPS-Seoul 2015 campaign.

Keywords: MAPS-Seoul 2015 campaign; Synoptic meteorological conditions; Long-range transport process.

INTRODUCTION

The latitude and longitude of the Korean Peninsula place it under prevailing westerlies, downwind of many Asian pollution sources. Previous studies have reported that the high levels of air pollutants in Korea are influenced not only by local emissions, but also by long-range transport (LRT) of pollutants from China (Davis and Jixiang, 2000; Lee *et al.*, 2001). Local emissions consistently occur over Korea throughout all seasons, whereas LRT of air pollutants mainly occurs during the spring (Liang *et al.*, 2004; Lin *et al.*, 2010; Lee *et al.*, 2014), therefore, trans-boundary transport from continental outflows is an important factor for the air quality of the Seoul Metropolitan Area (SMA), especially during the spring.

Meteorological processes determine the extent to which LRT air pollutants can contribute to degraded air quality over both the source and receptor areas, and have been previously reported as important factors (Levin *et al.*, 2005; Sun *et al.*, 2006; Wang *et al.*, 2006). This is because the impact of continental outflows from China has been evident over Northeast Asia and has become more frequent in recent years, therefore, extensive spatial and temporal extensive studies on emission source strength, meteorological conditions, and transport pathways are required to assess the contributions of transported pollutants accurately, especially for high-level air pollutant days in Korea.

In this context, the Korea-US Air Quality (KORUS-AQ) 2016 campaign (ttps://espo.nasa.gov/korus-aq/content/KORUS-AQ) has been planned in South Korea in collaboration with NASA and the USA scientific community for detailed field studies. In preparation for KORUS-AQ 2016

* Corresponding author.
Tel.: 82-51-510-3687; Fax: 82-51-515-1689
E-mail address: chkim2@pusan.ac.kr

campaign, a preliminary and a pilot field campaign, named the Megacity Air Pollution Studies-Seoul (MAPS-Seoul) 2015 campaign (https://espo.nasa.gov/sites/default/files/documents/MAPSSeoul_White%20Paper_26%20Feb%202015_Final.pdf), were designed, and a total of seven flights (RF1–RF7) were conducted from May 27–June 13, 2015, around the Korean Peninsula.

The purpose of this paper is to provide an overview of the meteorological conditions during the MAPS-Seoul 2015 campaign period by employing the following three synoptic meteorological applications. First, an explanation of the flight-by-flight synoptic summaries for each flight are provided. This includes an overview of the flight tracks and characteristics of the synoptic conditions during each flight, and investigates the meteorological conditions during the campaign period. Second, the mean streamline fields at the representative 850 hPa geopotential height level were analyzed to explain the meteorological characteristics affecting the LRT process during the campaign period. This is because the lower-tropospheric flow at around 1.5–3.0 km can be well characterized by LRT air pollutants, reflecting the influence of large semi-permanent anticyclones, as well as a less intense anticyclone over China. In addition, backward trajectory analysis has been conducted to identify the air mass origin based on the stagnant predominance (hereafter referred to as STG) case and LRT dominant mechanisms observed over the Korean Peninsula, and to determine the meteorological factors influencing LRT process and the chemistry of the trace species observed by the aircraft.

Lastly, several meteorological synoptic parameters were calculated to determine the unique meteorological features of each case during the campaign period. Jo *et al.* (2013) proposed 35 effective synoptic parameters for identifying and contrasting STG and LRT from the statistical tests, and suggested that 17 variables with p values of < 0.05 should be emphasized. The suggested 17 parameters include geostrophic wind speed, vorticity, vorticity advection at the 850 hPa geopotential level, and the vertical atmospheric stability index in the lower atmosphere showed classification accuracies of 93.2%, 87.8%, 85.4%, and 84.4%, respectively (Jo *et al.*, 2013). In this study, all of the 17 variables are employed to diagnose the meteorological characteristics relevant for distinguishing between the LRT and STG cases during the campaign period.

FLIGHTS TRACKS OF HANSEO KING-AIR-C90GT AIRCRAFT

During the MAPS-Seoul 2015 campaign period, a total of seven research flights of the Hanseo KingAir-C90GT aircraft (Textron Aviation Inc.) were conducted (from RF1 to RF7) from May to June 2015 around SMA, South Korea. A High-Resolution Time-of-Flight Aerosol Mass Spectrometer (HR-ToF-AMS, Aerodyne, Inc.) and an Ultra-High Sensitivity Aerosol Spectrometer (UHSAS, Droplet Measurement Technologies, Inc.) were on board the Hanseo KingAir-C90GT aircraft. Fig. 1 shows the surrounding flight area of the aircraft and major cities in South Korea. Each of the seven flight tracks and their altitudes in meters are presented in Fig. 2, and the flight information, including take-off, landing time, and flight paths, are summarized in Table 1. As would be expected, the research flights were mainly conducted along the west coastal area, over the YS, and around SMA (Table 1).

Among the seven flights, RF1 was a test flight; the remaining six followed several types of pathways in preparation for the KORUS-AQ 2016 campaign. RF3 and RF6 included spiral flights over the YS for the analysis of the vertical structure of aerosols collected in the marine atmosphere. RF5 mainly traveled over metropolitan cities, such as Gwangju, Busan, and other big urban areas, and then returned to Taean (base), as indicated in Fig. 1. RF4 and RF7 took off from the base, flew to Seoul and Wonju (Fig. 1) following similar paths, and sampled below 2500 m in altitude, before returning across the megacity (Table 1).

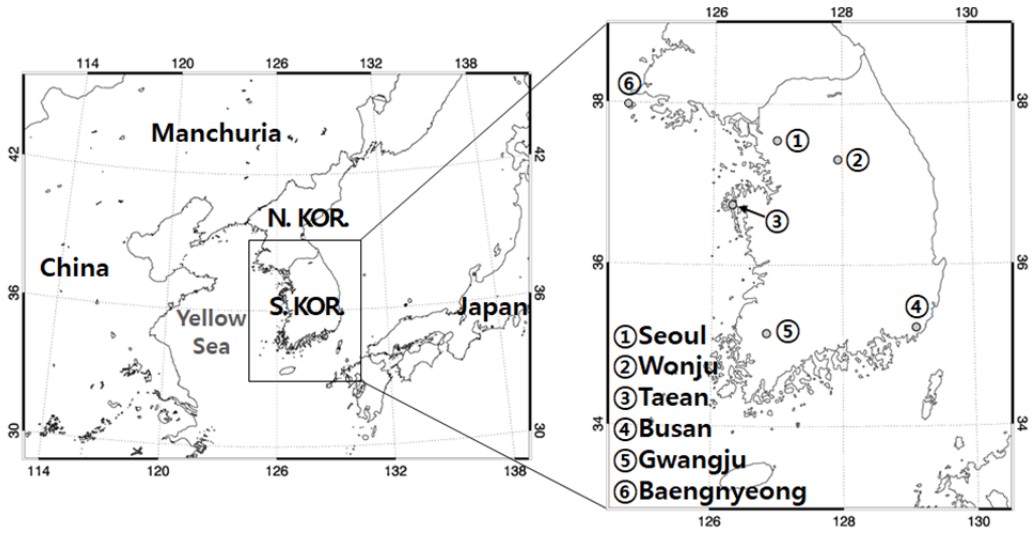

Fig. 1. Map of the area of the MAPS-Seoul 2015 campaign. The locations of the urban cities Taean (base), Seoul, Wonju, Busan, and Gwangju are denoted, through which the Hanseo KingAir-C90GT aircraft passed.

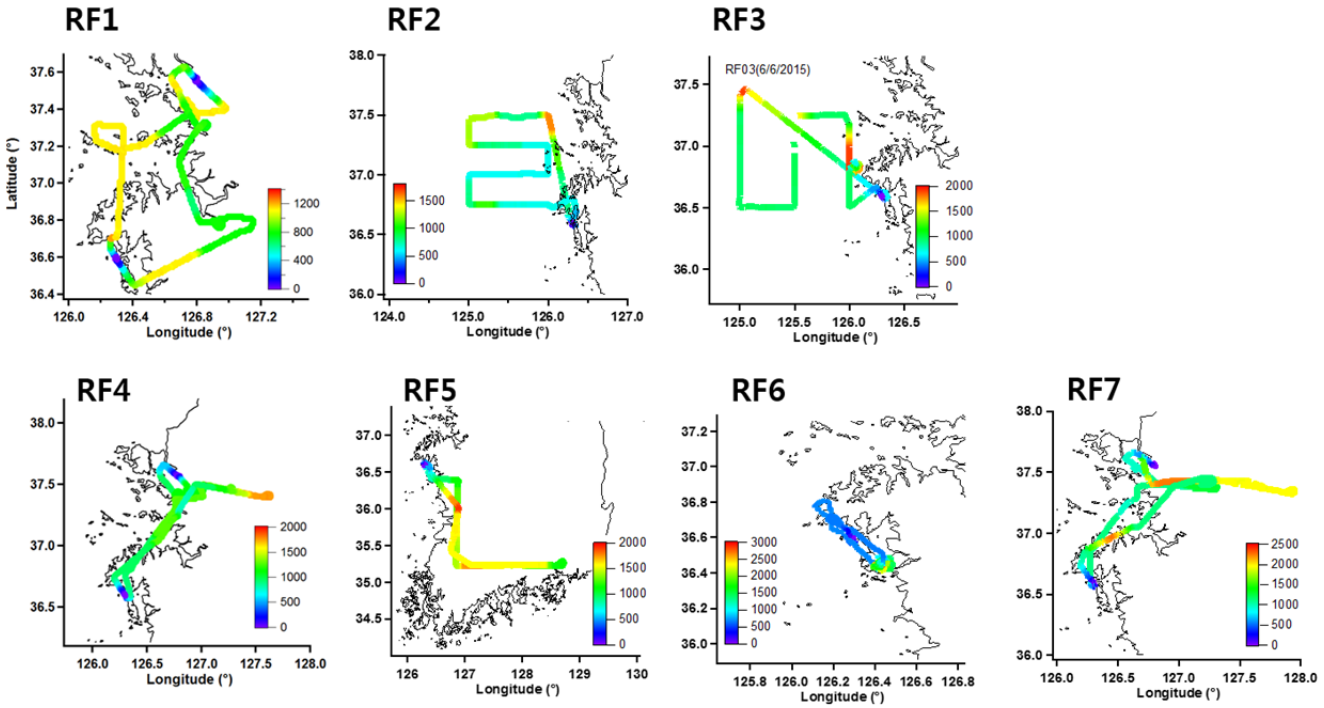

Fig. 2. The seven flight paths of the Hanseo KingAir-C90GT aircraft during the MAPS-Seoul 2015 campaign period. Color bar represents aircraft altitude in meter.

Table 1. Summary of the Hanseo KingAir-C90GT aircraft flights during the MAPS-2015 campaign.

RF	FLIGHT DATE	Take-off time (KST)	Landing time (KST)	FLIGHT PATH	REMARKS
RF1	27 May 2015	12:30	15:30	Southern SMA	Test flight without spiral flight
RF2	2 June 2015	16:00	18:30	Yellow Sea	Flight with different 2 heights
RF3	6 June 2015	14:00	17:00	Yellow Sea	Spiral flight was included
RF4	7 June 2015	09:30	12:30	Coastal + Urban area	Taean-Seoul-Wonju-Taean
RF5	7 June 2015	13:30	16:30	Urban area	Taean-Gwangju-Busan-Gwangju-Taean
RF6	13 June 2015	09:30	11:30	Yellow Sea	Spiral flight was included
RF7	13 June 2015	13:30	17:00	Coastal + Urban area	Taean-Seoul-Wonju-Taean

FLIGHT-BY-FLIGHT SYNOPTIC SUMMARIES

The synoptic characteristics for all seven flights are summarized in this section, providing synoptic features for each flight day. The signatures of the LRT processes from the weather maps are discussed here. The weather maps (Fig. 3), and streamline charts with isotach (Fig. 4) are acquired from the Korea Meteorological Administration (KMA) web site (http://www.weather.go.kr/weather/images/analysischart.jsp). It should be also noted that there was no Asian dust recorded, nor wildfire occurrences reported during the campaign period. Other specific biases of both natural and anthropogenic emissions are not reported.

Flight 1 (RF1); May 27, 2015 (1230–1550 KST)

RF1 was the initial survey flight around the SMA. In the 850 hPa geopotential level synoptic map (Fig. 3(a)), a high-pressure system dominated during the first flight, creating strong STG conditions over the Korean Peninsula and the adjacent areas in the ocean south of the Peninsula. Under the blocking anticyclone, wind fields do not show the features of the LRT process of air pollutants from China to the Korean Peninsula, and only show weak wind fields with stagnant high pressure over Northeast Asia. Therefore, the day of Flight 1 can be classified as one of the typical STG cases identified among the seven flights.

Streamlines are governed by the stagnant and quasi-stationary anticyclone system with veering (change in wind direction clockwise) circulations located over the Korean Peninsula (Fig. 4(a)). The veering circulations prevailed over the center of the stagnating, slowly migrating anticyclone, and were expected to be persistently transporting air from the upper to the lower atmosphere. Whereas, it is expected that this horizontally blocks the downwind transport of air pollutants from China to the Korean Peninsula.

Flight 2 (RF2); June 2, 2015 (1600–1830 KST)

Under the presence of both broad and weak low pressure over North Korea and high pressure over northwest China, the wind fields showed overall low northwesterlies at 850 hPa

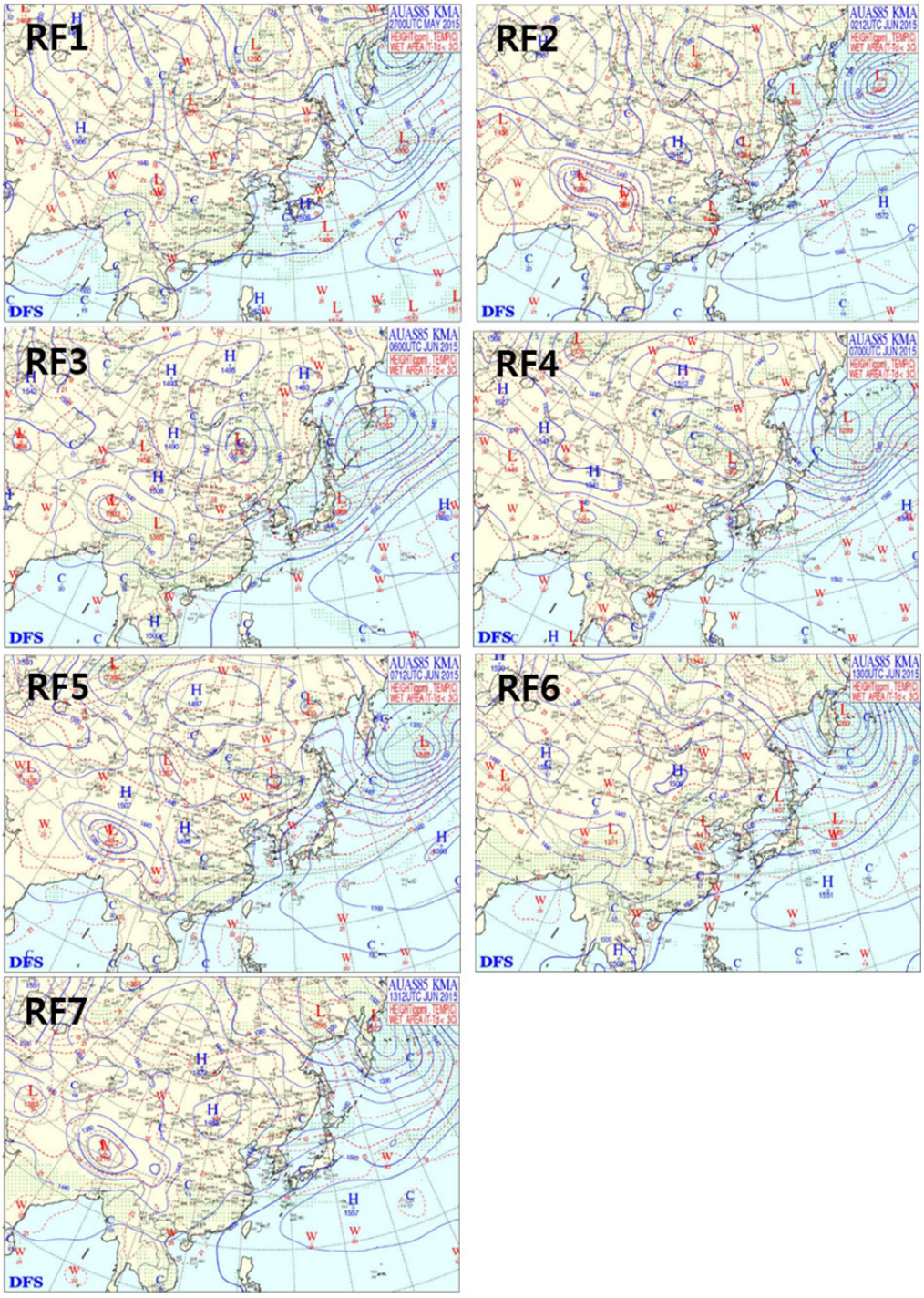

Fig. 3. Synoptic weather chart at 850 hPa for the seven flights during the MAPS-Seoul 2015 campaign period. Images are acquired via website (http://www.weather.go.kr/weather/ images/analysischart.jsp).

in and around the Korean Peninsula (Fig. 3(b)), with no noticeable indicators of the LRT process. The streamline also showed that the low northwesterlies (or northerlies) only prevailed over the YS (Fig. 5(b)), but there were no particular wind field features over the Korean Peninsula, which experienced only weak or lower wind speed (Fig. 4(b)). Therefore, the day of the RF2 could be also described as an STG case over the Korean Peninsula, with mostly local emissions contributions to the air quality over urban Korean cities due to the stagnant conditions over Korean Peninsula. Excluding the low wind speed over inland Korea, strong northwesterlies (or northerlies) prevailed over the YS during the RF2, as indicated in Fig. 5(b). The northerlies prevailing over the YS were due to high pressure in northeastern China and low pressure in northern North Korea (Fig. 4(b)), resulting in a pressure gradient force leading the wind direction northeasterly from northeastern China to the YS. This streamline pattern (Fig. 5(b)) is

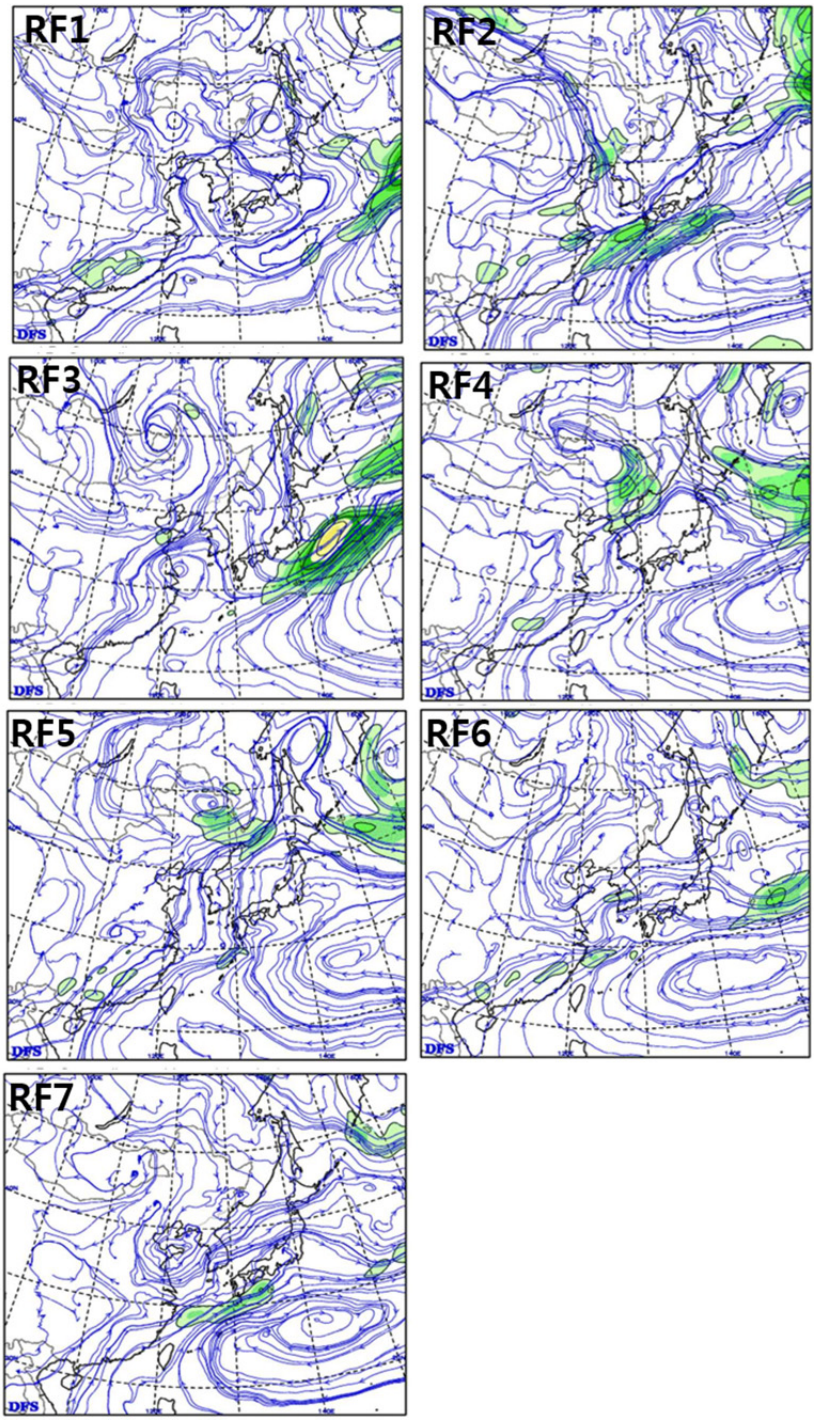

Fig. 4. Streamlines and Isotach (> 25 knots) at 850 hPa for the seven flight cases. Images are acquired via the website (http://www.weather.go.kr/weather/images/analysischart.jsp).

expected to be conducive to the LRT process from northern China (Manchuria) toward the YS, however, the effect was not expected to be significant because of the geographical location of Manchuria, the remote area from high anthropogenic emission regions.

Flight 3 (RF3); June 6, 2015 (1400–1700 KST)

The wind fields over the Korean Peninsula were governed by a strong migratory low-pressure system located over northern China. The characteristics of the wind fields can be described as two distinctive features from the geographical viewpoint of the YS: confluent flow over the entrance of the YS, and diffluent flows from the exit of the YS towards the Korean Peninsula (Fig. 3(c)). Two confluent flows originating from central and southern China converge, creating convergent wind fields around the entrance of the YS, enabling long-range transport from both Beijing and Shanghai into the YS. Over the YS, northwesterlies and

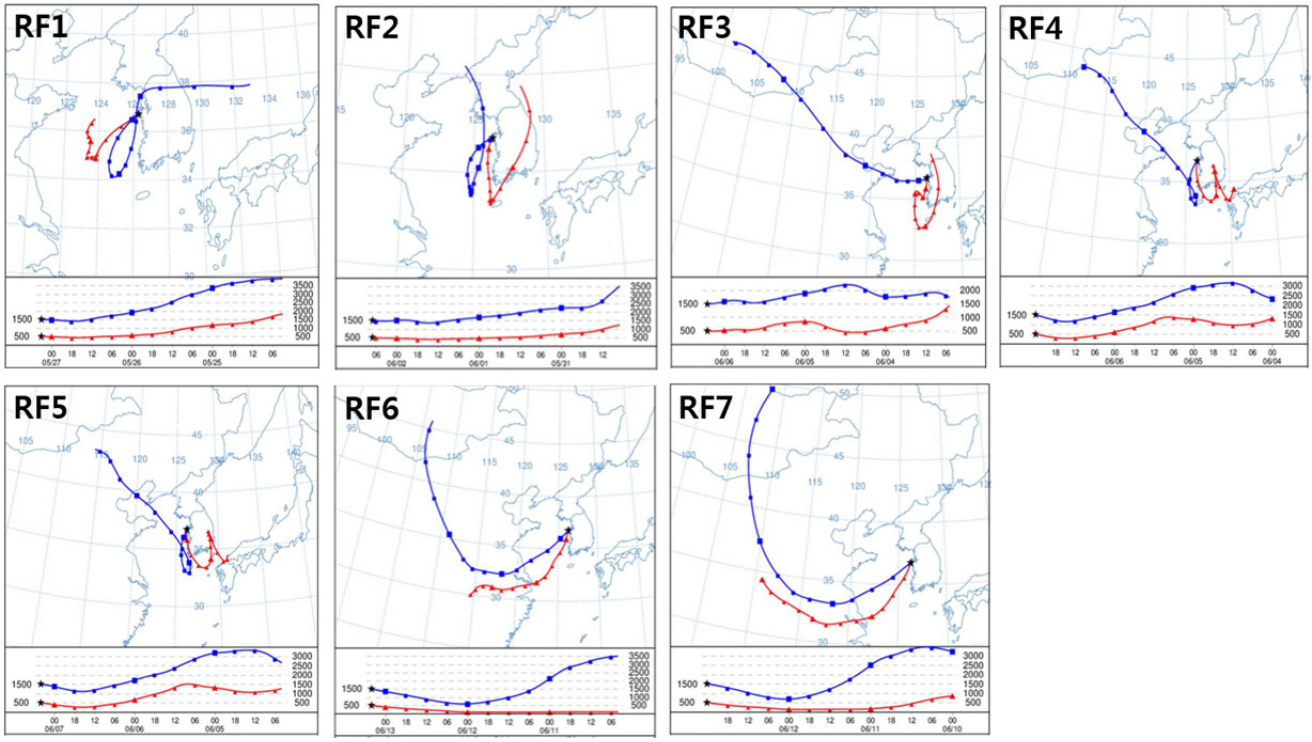

Fig. 5. Three-day backward trajectories starting at Taean (base) at 500 m and 1500 m from the take-off times of the seven flights.

westerlies were predominantly driven due to pressure gradients caused by the flank of migratory low pressure over both northeastern and southeastern China.

Over the exit of the YS and the western coastal area of the Korean Peninsula, divergence of winds created the diffluent wind fields, hindering the penetration of LRT process towards inland Korean Peninsula from the YS (Fig. 4(c)). As a result, lower westerlies, or weak wind speeds with backing (change in wind direction anti-clockwise) circulation, were identified over inland Korea, and do not continue to extend to inland Korean Peninsula, especially in the afternoon. Only a broad, stagnant pressure system prevailed over the surface of inland Korean Peninsula, while there was noticeable evidence of LRT prevailing over the YS and western coast of Korean Peninsula.

Flight 4 (RF4); June 7, 2015 (0930–1230 KST)

The synoptic situation did not differ much from that of RF3, with the exception of the location of an extensive migratory low pressure over Manchuria, which slowly progressed towards the Korean Peninsula (Fig. 3(d)). Similar to RF3 case, Korean Peninsula was influenced by the flank of a cyclone located over Manchuria with weaker westerlies over the whole Korean Peninsula than those during Flight 3. The wind speed of the streamline was also weaker over South Korea, except for small (but not significant) transport signals from southwest China to the YS at the 1.5-km geopotential height level (Fig. 5(d)). Therefore, during the period of RF4, a broad stagnant pressure system prevailed at the lower atmosphere, which can be defined as an STG case, while LRT processes at a geopotential height of 1.5 km or higher were expected, however, these would be weaker than those during RF3 (Fig. 5(d)).

Flight 5 (RF5); June 7, 2015 (1330–1630 KST)

During RF5, the synoptic situation did not differ greatly from that during RF4, excluding a small, migratory high-pressure system arising over central China. As the high-pressure system slowly moved eastwards, the resultant prevailing winds over both the YS and the Korean Peninsula slowly shifted direction, from westerlies to southwesterlies. The similar transport signals were identified over both the YS and inland South Korea (see Figs. 3(e) and 4(e)), with the process of producing some LRT signals during the RF5, especially at a geopotential height level of 850 hPa. However, considering the southwesterlies, carrying clean air from the southern marine atmosphere that cleans and purges high air pollution over the Korean Peninsula can be transported, and therefore LRT from high emission areas, such as urban cities in China, is expected to be negligible.

Flight 6 (RF6); June 7, 2015 (0930–1230 KST)

A migratory cyclone prevailed over North Korea, with prevailing zonal flows from the anti-cyclone located over eastern Japan (Fig. 3(f)). Under the high-pressure conditions located over the southeastern marine area of South Korea and Japan, strong zonal wind speed was expected with the favorable condition of strong LRT process over the whole Korean Peninsula. These synoptic conditions induced strong LRT processes from central and southern China in both the upper and lower atmosphere. Thus, it is expected that these conditions would influence the air pollution level in both

the YS and urban cities in South Korea. Streamlines on June 7, 0900 KST (00 UTC) created meteorological conditions (Fig. 4(f)) that favored the LRT processes.

Flight 7 (RF7); June 7, 2015 (1330–1700 KST)

The synoptic situation during RF7 did not differ much from that during RF6, showing the condition of LRT over the Korean Peninsula, with the exception of the fact that the migratory cyclone that prevailed over North Korea had completely dissipated (Figs. 3(g) and 4(g)). Overall, the same features present during RF6, such as the zonal wind speed over the Korean Peninsula, were found, and these resulted in high probabilities of LRT from central and southern China in both the upper and lower atmosphere due to the westerlies or southwesterlies blowing directly towards the Korean Peninsula, then moving towards Japan and the Pacific Ocean.

TRAJECTORY ANALYSIS

Backward trajectory analyses have a wide range of applications in the atmospheric and air quality fields as they can be used to identify transport pathways affecting a study site by describing the recent meteorological history of an air mass, and then determine potential sources of air tracers. In the current study, describing the recent meteorological histories of an air masses during or after aircraft surveying is highly important as the synoptic systems that develop over China often pass over the Korean Peninsula, especially during the spring. We conducted three-day backward trajectories for each of the seven flights as the time scale from developing a synoptic system in China to it reaching the Korean Peninsula is approximately three days (Park *et al.*, 2002). Thus, 72-hour backward trajectories were computed here at the starting time of each of the seven flights, based on the Hybrid Single-Particle Lagrangian Integrated Trajectory (HYSPLIT) dispersion model v4 (June 2015) (Draxler and Rolph, 2003).

The backward trajectories, beginning at Taean (Fig. 1), were analyzed, and the time spent by the air parcels over different influential regions before reaching the Taean at two given heights (500 and 1500 m) at the flight departure time are presented in Table 1. We expected that these two heights would represent the most frequent height of LRT process from China, and the typical height of the surface air, respectively. Analysis was conducted by determining the hourly coordinates (latitude and longitude) of the trajectories. Input data for HYSPLIT-4 were the final analysis (FNL) 6-hour archived meteorological data from the National Centers for Environmental Prediction–National Center for Atmospheric Research (NCEP–NCAR).

Fig. 5 depicts backward trajectories for each of the seven flights. The results of RF1 and RF2 revealed that the air flows reaching the Taean show no features of the LRT process due to the weak wind speed under stagnant synoptic conditions (Fig. 5), indicating that most of the monitoring data originated from the local emissions of urban cities in the Korean Peninsula.

However, the trajectories of RF3 starting at 1500 km showed clear evidence of LRT, as indicated by the westerlies, especially those over the YS. The LRT process was expected to originate from northeastern China or Mongolia (Fig. 5). However, the trajectory starting in the lower atmosphere (i.e., 500 m) shows the influence of a broad stagnant pressure system that prevailed over the surface and lower atmosphere of the Korean Peninsula, with no evidence of LRT at the surface, simply generating complicated meteorological features. However, considering the height of LRT process over Northeast Asia, RF3 can be classified as one of the possible LRT cases among the seven flights.

RF4 and RF5 show similar patterns to RF3, with long- or medium-range transport processes at 1.5 km, however, all of the backward trajectories starting at 1.5 km during RF4 and RF5 were complicated, as they were traced to the southern coastal urban cities prior to transport from the southern marine atmosphere. Therefore, it is difficult to classify the patterns identified during RF4 and RF5 into either STG or LRT. Only found were conditions that favored local emissions prevailed over the surface and in the lower atmosphere (Fig. 5).

RF6 and RF7 show strong LRT processes in both the upper and lower atmosphere, originating from central China in the lower atmosphere, and central and northern China or Mongolia in the upper atmosphere, due to the westerly and northwesterly wind fields blowing towards the Korean Peninsula, respectively.

SYNOPTIC METEOROLOGICAL PARAMETERS

Jo *et al.* (2013) calculated numerous daily-mean synoptic meteorological parameters from both STG and LRT cases, and suggested 17 synoptic scale variables as indicators for classification as STG- and LRT-dominant cases. In this study, all of the suggested 17 synoptic meteorological parameters were calculated during the MAPS-Seoul 2015 campaign period.

The synoptic meteorological data employed in the current study is NCEP Final (FNL) analysis data which has a resolution of 1 degree × 1 degree resolution, and the synoptic meteorological parameters for each of the seven flight cases were assessed to determine which characteristics dominate in either STG or LRT cases. Numbers of synoptic meteorological parameters have been used for air pollution source diagnosis in previous studies (Dobbins, 1979; Sanchez *et al.*, 1990; Davis and Gay, 1993), and these synoptic variables together with additional ones were assessed and 17 parameters were suggested by Jo *et al.* (2013). The suggested parameters include geostrophic wind speed, vorticity, vorticity advection, and geostrophic wind speed at a geopotential height of 850 hPa, the vertical stability index for the lower atmosphere, and other humidity- or pressure-related parameters.

Table 2 presents the 17 meteorological variables, and Fig. 6 shows the ranges of selected variables. Also daily mean ground-based PM_{10} mass concentrations observed at two sites, Baengnyeong (island site) and Seoul (SMA site), were also indicated in Fig. 6(a). It should be noted that

Table 2. List of the synoptic meteorological parameters calculated for the periods of the seven flights during the MAPS-Seoul 2015 campaign period.

Variables	Explanation	RF1	RF2	RF3	RF4	RF5	RF6	RF7
$\lvert\vec{V}_g\rvert_{850}$	850-hPa geostrophic wind speed (m s^{-1})	3.9	2.3	9.6	7.0	5.9	13.3	12.1
ζ_{850}	0000 UTC 850-hPa vorticity (s^{-1})	-2.4×10^{-5}	6.6×10^{-6}	-2.4×10^{-5}	-5.6×10^{-5}	-4.0×10^{-5}	4.0×10^{-5}	9.1×10^{-6}
$\vec{V} \cdot \nabla\zeta_{850}$	850-hPa vorticity advection (s^{-2})	7.7×10^{-11}	-5.1×10^{-10}	4.7×10^{-10}	-2.8×10^{-10}	-2.3×10^{-10}	4.1×10^{-10}	1.5×10^{-9}
S	Vertical stability index of lower atmosphere (°C)	–6.7	–2.9	–5.5	–5.2	–4.4	–3.7	–3.7
$T_{\sigma\text{-}00}$	0000 UTC surface dewpoint temperature (K)	283.7	287.4	288.4	287.4	287.2	291.3	291.5
RH_m	Daily mean surface relative humidity (%)	58.9	77.9	79.4	79.0	79.0	90.3	90.3
RH_{eff}	Daily mean surface effective humidity (%)	43.9	50.4	49.4	51.6	51.6	56.5	56.5
T_{min}	Surface mean temperature (K)	287.6	289 .6	289.9	289.8	289.8	291.2	291.2
Ps_{00}	0000 UTC surface pressure (hPa)	1010.3	1008.5	1012.9	1014.5	1013.0	1004.2	1004.6
ED_{00}	0000 UTC ED for surface-850-hPa (K km^{-1})	0.0	0.0	–0.1	–0.1	–0.2	0.0	0.1
EDI_{00}	0000 UTC EDI for surface-850-hPa (K)	4.4	2.0	–0.6	0.5	0.3	0.5	1.1
ΔM_{500}	500-hPa Montgomery dry potential change (J kg^{-1})	3.2×10^4	3.2×10^4	2.6×10^4	2.6×10^4	2.8×10^4	2.4×10^4	2.4×10^4
ΔMS_{850}	850-hPa moist static energy change (J kg^{-1})	1.5×10^4	1.4×10^4	1.3×10^4	1.3×10^4	1.2×10^4	1.5×10^4	1.6×10^4
W_{mean}	Daily mean surface wind speed (m s^{-1})	2.2	4.6	7.2	2.9	2.9	6.2	6.2
M_{850}	0000 UTC 850-hPa Montgomery dry potential (J kg^{-1})	3.0×10^5	3.0×10^5	3.0×10^5	3.0×10^5	3.0×10^5	3.1×10^5	3.1×10^5
ζ_{500}	0000 UTC 500-hPa vorticity (s^{-1})	-2.1×10^{-6}	-2.4×10^{-6}	-2.6×10^{-5}	-1.1×10^{-5}	-9.9×10^{-6}	-2.0×10^{-5}	-1.0×10^{-5}
$\vec{V} \cdot \nabla\zeta_{850}$	500-hPa vorticity advection (s^{-2})	-2.5×10^{-9}	-1.7×10^{-9}	-2.3×10^{-10}	-3.1×10^{-10}	-1.0×10^{-10}	4.0×10^{-10}	-7.6×10^{-10}

Baengyeong and Seoul sites are representing background and typical urban areas, respectively. The PM_{10} observations at two sites were acquired from web site (http://www.airkorea.or.kr/index). In Table 2 and Fig. 6, vorticity ($\zeta = \frac{\partial v}{\partial x} - \frac{\partial u}{\partial y}$), vorticity advection ($\vec{V} \cdot \nabla\zeta = u\frac{\partial\zeta}{\partial x} + v\frac{\partial\zeta}{\partial y}$), and geostrophic wind speed ($|\vec{V}_g| = \left(u_g^2 + v_g^2\right)^{1/2}$) were calculated at 36.5°N, 126.5°E, an approximate location of the Tean (Fig. 1), using four nearby grid points from NCEP-FNL data which has a resolution of 1 degree × 1 degree. The humidity index (EDI = T – T_d between surface and 850 hPa, where T and T_d are temperature and dew temperature, respectively) (Davis and Gay 1993) is an indicator of potential precipitation. The Montgomery dry potential ($M = c_pT + gH$), moist static energy ($Ms = c_pT + g{\cdot}H + L{\cdot}q$), and effective humidity ($RH_{eff} = 0.3\ (RH_d + 0.7\ RH_{d\text{-}1} + 0.7^2\ RH_{d\text{-}2})$) were also used, where c_p represents the specific heat at a constant pressure, g is gravitational acceleration, H is geopotential height, L is latent heat, q is mixing ratio, RH is relative humidity, and d-*i* is the i^{th} day prior to the indicated day. The vertical stability index of the lower atmosphere (S) represents the temperature lapse rate between geopotential height fields of 1000 hPa and 850 hPa, and is defined as T2 minus T1, where T1 and T2 are the temperatures at 1000 hPa and 850 hPa, respectively.

Jo *et al.* (2013) showed that the most suitable variables for separation of LRT and STG cases were the following dynamic meteorological parameters: geostrophic wind speed ($|\vec{V}_g|_{850}$), vorticity (ζ_{850}), and vorticity advection ($\vec{V} \cdot \nabla\xi_{850}$) at a geopotential height of 850 hPa, with estimated classification accuracies of 93.2%, 87.8%, and 84.4%. It is unsurprising that geostrophic wind speed is the most important variable for distinguishing between the two types of days: STG and LRT cases. The LRT-dominant cases were associated with stronger $|\vec{V}_g|$, (+) negative ζ_{850}, and higher vorticity advection ($\vec{V} \cdot \nabla\xi_{850}$), while STG-dominated days were associated with lower $|\vec{V}_g|$, (–) negative ζ_{850}, and lower vorticity advection ($\vec{V} \cdot \nabla\xi_{850}$). The lower atmosphere stability index (S) was positive (stable) for the STG cases, with weak geostrophic wind speeds, while for the LRT cases, S was negative (unstable), with strong geostrophic wind speeds. Humidity-related indices, such as RH_{eff}, RH_m, and EDI, were found to be drier for the LRT cases than those for the STG cases (Jo *et al.*, 2013)

The geostrophic wind speeds during RF1 and RF2 were found to be lower (stagnant cases), at 3.9 and 2.3 m s^{-1}, respectively, while those during RF3, RF6, and RF7 indicated LRT features, at 9.6, 13.3, and 12.1 m s^{-1}, respectively (Table 2 and Fig. 6), suggesting that geostrophic wind speed is a basic and novel indicator of LRT. The vorticity at 850 hPa also showed that RF1 was a stagnant case, with (–) negative vorticity values, while higher (+) positive values were found during RF6 and RF7, indicating LRT features, showing synonymous result with that of Jo *et al.* (2013). On other days, synoptic conditions were more

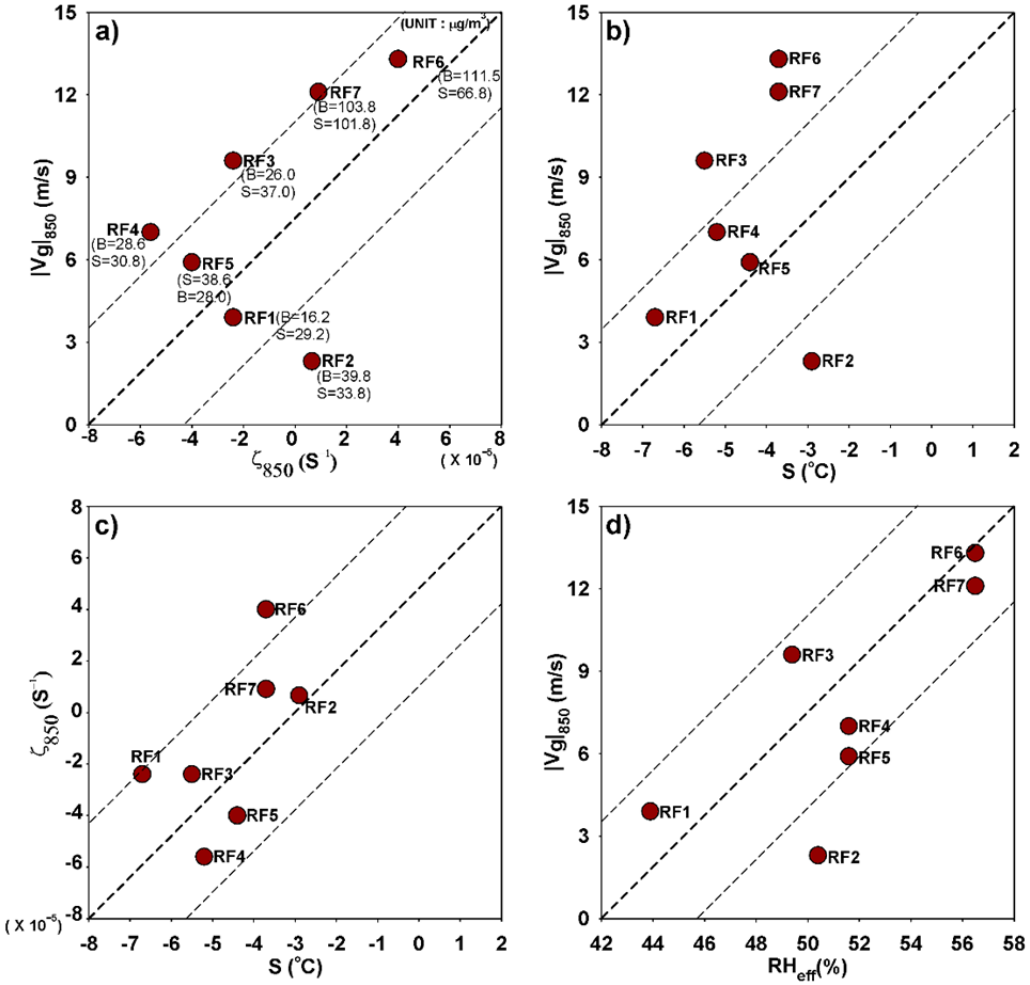

Fig. 6. Ranges of the selected synoptic meteorological parameters calculated for the periods of the seven flights (RF1–RF7) during the MAPS-Seoul 2015 campaign period. In-situ measurements of PM_{10} mass concentrations observed at two sites during the campaign period, Baengnyeong and Seoul, are also indicated in Fig. 6(a).

complicated, but vorticity advection was smaller during RF1, RF4, and RF5 ranging approximately from -5.6×10^{-5} to -2.4×10^{-5} s^{-1}, suggesting that these were likely to be STG cases.

The tendencies of the lower atmosphere stability index (S), RH_{eff}, RH_m, and EDI were also indicated in Table 2. The lowest values of S were found for RF1 (–6.7°C), and the highest were identified for RF2 (–2.9°C), indicating that the atmospheric stability conditions were unstable for all of the RF1–RF7 (Table 2 and Fig. 6). The highest S value for RF2 suggested the tendency of STG case among total seven flight days. Humidity indices, such as RH_{eff} and RH_m, were the lowest for RF1, with values of 43.9% and 58.9 % for RF_{eff} and RH_m, respectively, and the highest for RF6 and RF7, with values of 56.5%, and 90.3 % for RF_{eff} and RH_m, respectively. It is noted that RF6 and RF7 that showed the features of LRT cases showed higher humidity, the opposite sign of humidity for the MAPS-Seoul 2015 campaign period, compared with those in Jo *et al.* (2013).

Other parameters, such as surface dew point temperature ($T_{\sigma\text{-}00}$), surface minimum temperature (T_{min}), surface pressure (Ps_{00}), ED_{00}, and EDI_{00}, which are mostly thermodynamic or humidity parameter groups, showed the similar tendencies, with higher pressure and more stable conditions favoring STG cases with short-distance trajectories, as indicated in Fig. 5. These results further suggest that RF1 and RF2, and RF5 to some extent, were STG cases, while RF3, RF6, and RF7 were LRT cases, as shown in Table 2.

The synoptic meteorological conditions discussed above can be summarized as follows: RF1 and RF2 can be classified as STG cases, enabled by weak ventilation effects and slower pollutant transport processes under the prevailing stagnant pressure system. Vorticity was negative for both RF1 and RF2, with geostrophic wind speeds of less than 5 m s^{-1} in the lower atmosphere (850 hPa), and these flights were characterized by relatively drier conditions. Complicated characteristics were identified for RF4 and RF5, identifying both STG and LRT processes. RF4 showed shifted LRT characteristics, with stronger geostrophic wind speeds of 7.0 m s^{-1}, but slightly lower or approximately the same S of –5.2°C as that of RF5.

LRT characteristics were clear during RF3, RF6, and RF7, and they were influenced by LRT effects from China, which were well characterized by positive vorticity and

strong geostrophic wind speeds of 9.6–13.3 m s^{-1} over the Korean peninsula. The anticyclone that prevailed during the LRT cases favored the maintenance of a strong pressure gradient, and the resultant westerlies could transport pollutants emitted from central (or northern) China towards the Korean Peninsula.

We also analyzed in-situ measurements of PM concentrations at two sites: Baengnyeong and Seoul. PM data was downloaded from web site: http://www.airkorea.or.kr/. It should be noted that unfortunately no adequate quantitative data on $PM_{2.5}$ concentrations are available during the campaign period. Instead we analyzed in-situ measurements of PM_{10} mass concentrations at two sites, Baengnyeong and Seoul, obtained from web site: http://www.airkorea.or.kr/index, and indicated in Fig. (6a). The observed daily mean PM_{10} concentrations (Fig. 6(a)) were 111.5 μg m^{-3} in Baengnyeong (Seoul: 66.8 μg m^{-3}) for RF6, and 101.8 μg m^{-3} at Seoul (Baengnyeong: 101.8 μg m^{-3}) for RF7, the highest levels recorded at each of the two sites during the whole MAPS-Seoul 2016 campaign period due to the LRT process over the west coastal or marine area.

Fig. 7 shows diurnal variations of wind vectors observed at two sites, Baengnyeong and Seoul, which were obtained from the KMA website (https://data.kma.go.kr/cmmn/main.do). As in Fig. 7, wind speed during the RF1 and RF2 showed relatively lower than others at both sites, indicating the possible STG features, as described above. However, during RF3, wind vectors at Baengnyeong showed stronger westerlies (or northwesterlies), whereas those observed at Seoul showed weak ones. For RF4–RF5, northerlies prevailed at surface in the marine atmosphere, thereby suggesting no impact from Chinese emissions. However, stronger westerlies (or southwesterlies) were found at Baengnyeong during RF6–RF7, with the wind speed of more than > 5 m s^{-1}, implying possibilities of LRT of air pollutants transported from inland China. In particular, the observed wind directions at Seoul, easterlies or northeasterlies, showed the opposite in wind direction compared with those at Baengnyeong, westerlies or southwesterlies. This is implying that the predominance of LRT process in the marine atmosphere plus convergence of wind fields, are resulting to higher PM concentrations in SMA due to the little ventilation and lower possibility of transport toward outer region of Korean Peninsula.

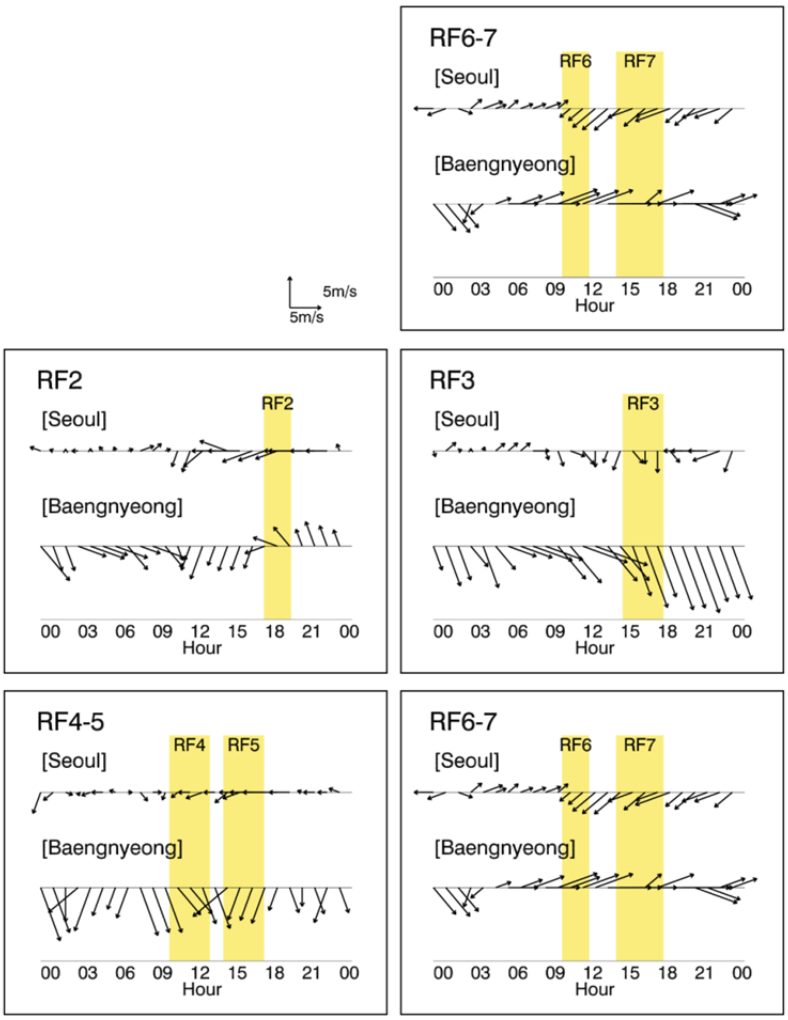

Fig. 7. Diurnal variations of wind vectors observed at two sites, Baengnyeong and Seoul, obtained from the KMA web site (https://data.kma.go.kr/cmmn/main.do).

CONCLUSION

We discussed meteorological analyses for each of the seven flights conducted during the MAPS-Seoul 2015 campaign (May 27–June 13). Streamline and trajectory analyses were also presented to classify the periods of the seven flights into two types of transport processes: prevailing stagnant or long-range transport. The results showed that the conditions during all seven of the cases were governed by migratory cyclone and/or anticyclone systems located over Northeast Asia. Streamlines were also governed by the stagnant and quasi-stationary anticyclone systems located near the Korean Peninsula, with veering/backing circulations of wind fields.

From the analyses of both synoptic maps and backward trajectories, RF1 and RF2 showed stagnant synoptic conditions, and long-range transport processes were observed in RF3, RF6, and RF7. Complicated characteristics were displayed during RF4 and RF5, with both stagnant and long-range transport features from the southern marine atmosphere and no long-range transport processes from high-emission Chinese cities.

In addition, 17 synoptic meteorological variables, as diagnostic indicators of long-range transport processes, were applied to the seven flight cases. The results again showed lower geostrophic wind speeds (stagnant cases) of 3.9 and 2.3 m s^{-1} for RF1 and RF2, respectively, while those of RF3, RF6, and RF7 exhibited values (long-range transport cases) of 9.6, 13.3, and 12.1 m s^{-1}, respectively. The indicated vorticity for RF1 at 850 hPa was (–) negative, while the values for RF6 and RF7 (long-range transport days) were high and (+) positive, with both sites displaying the highest observed PM_{10} concentrations of the whole campaign: 111.5 μg m^{-3} over the Yellow Sea (RF6) and 101.8 μg m^{-3} at the Seoul site (RF7). Other parameters followed the same tendencies of stagnant and long-range transport processes; however, characteristics of both were observed during RF4 and RF5, making it difficult to distinguish between the two types.

The meteorological variables described above can be used to determine the background concentrations around the Korean Peninsula during the formation of some of the more notable trace atmospheric constituents observed during the MAPS-Seoul 2015 campaign. Several of these constituents will be discussed in future MAPS-Seoul 2015 campaign papers in relation to the meteorological features explained here. During this analysis process, important signatures will also be provided in the assessment of different combinations of source strength, transport patterns, and removal mechanisms applicable to the various species measured during the campaign, enabling the characterization of chemical signatures, which can also be used to assess the air masses through which these flights passed.

ACKNOWLEDGEMENT

We thank National Institute of Environmental Research (NIER) for providing the MAPS-Seoul 2015 campaign measurements, and also thank KMA for providing meteorological observation data and numbers of synoptic weather charts. In addition, J.-J. Lee, and H.-J. Lee acknowledge supports made by National Research Foundation of Korea (NRF) funded by the Ministry of Education (NRF-2015R1D1A1A01059576), and (NRF-2015R1D1A1A01060088), respectively.

REFERENCE

Davis, B.L. and Jixiang, G. (2000). Airborne particulate study in five cities of China. *Atmos. Environ.* 34: 2703–2711.

Davis, R.E. and Gay, D.A. (1993). A synoptic climatological analysis of air quality in the Grand Canyon National Park. *Atmos. Environ.* 5: 713–727.

Dobbins, R.A. (1979). *Atmospheric motion and air pollution: An introduction for students of engineering and science*. John Wiley and Sons, 344 pp.

Draxler, R.R. and Rolph, G.D. (2003). HYSPLIT—Hybrid Single-Particle Lagrangian Integrated Trajectory Model. NOAA Air Resources Laboratory. http://ready.arl.noaa.gov/HYSPLIT.php.

Jo, H.Y. and Kim, C.H. (2013). Identification of long-range transported haze phenomena and their meteorological features over Northeast Asia. *J. Appl. Meteor. Climatol.* 52: 1318–1328.

Kim, C.H., Park, S.Y., Kim, Y.J., Chang, L.S., Song, S.K., Moon, Y.S. and Song, C.K. (2012). A numerical study on indicators of long-range transport potential for anthropogenic particulate matters over Northeast Asia. *Atmos. Environ.* 58: 35–44.

Lee, H.J., Kim, S.W., Brioude, J., Cooper, O.R., Frost, G.J., Kim, C.H., Park, R.J., Trainer, M. and Woo, J.H. (2014). Transport of NO_x in East Asia identified by satellite and in situ measurements and Lagrangian particle dispersion model simulations. *J. Geophys. Res.* 119: 2574–2596.

Lee, J.H., Kim, Y.P., Moon, K.C., Kim, H.K. and Lee, C.B. (2001). Fine particle measurements at two background sites in Korea between 1996 and 1997. *Atmos. Environ.* 35: 635–643.

Levin, Z., Gershon, H. and Ganor, E. (2005). Vertical distribution of physical and chemical properties of haze particles in the Dead Sea valley. *Atmos. Environ.* 39: 4937–4945.

Liang, Q., Jaeglé, L., Jaffe, D.A., Weiss-Penzias, P., Heckman, A. and Snow, J.A. (2004). Long-range transport of Asian pollution to the northeast Pacific: Seasonal variations and transport pathways of carbon monoxide. *J. Geophys. Res.* 109: D23S07.

Lin, M., Holloway, T., Carmichael, G.R. and Fiore, A.M. (2010). Quantifying pollution inflow and outflow over East Asia in spring with regional and global models. *Atmos. Chem. Phys.* 10: 4221–4239.

Park, S.U., Lee, Y.H. and Lee, E.H. (2002). Estimation of nitrogen dry deposition in South Korea. *Atmos. Environ.* 36: 4951–4964.

Sanchez, M.L., Pascual, D., Ramos, C. and Perez, I. (1990). Forecasting particulate pollutant concentrations

in a city from meteorological variables and regional weather patterns. *Atmos. Environ.* 6: 1509–1519.

Sun, Y., Zhuang, G., Tang, A., Wang, Y. and An, Z. (2006). Chemical characteristics of $PM_{2.5}$ and PM_{10} in haze-fog episodes in Beijing. *Environ. Sci. Technol.* 40: 3148–3155.

Wang, Y., Zhuang, G., Sun, Y. and An, Z. (2006). The variation of characteristics and formation mechanisms of aerosols in dust, haze, and clear days in Beijing. *Atmos. Environ.* 40: 6579–6591.

Received for review, October 30, 2017
Revised, March 31, 2018
Accepted, May 9, 2018